

## Partial disruption of a planet around a white dwarf: the effect of perturbation from the remnant planet on the accretion

ABDUSATTAR KURBAN <sup>1,2,3</sup> XIA ZHOU <sup>1,2,3</sup> NA WANG <sup>1,2,3</sup> YONG-FENG HUANG <sup>4,5,1</sup> YU-BIN WANG <sup>6</sup> AND  
NURIMANGUL NURMAMAT <sup>4</sup>

<sup>1</sup>*Xinjiang Astronomical Observatory, Chinese Academy of Sciences, Urumqi 830011, Xinjiang, People's Republic of China*

<sup>2</sup>*Key Laboratory of Radio Astronomy, Chinese Academy of Sciences, Urumqi 830011, Xinjiang, People's Republic of China*

<sup>3</sup>*Xinjiang Key Laboratory of Radio Astrophysics, Urumqi 830011, Xinjiang, People's Republic of China*

<sup>4</sup>*School of Astronomy and Space Science, Nanjing University, Nanjing 210023, People's Republic of China*

<sup>5</sup>*Key Laboratory of Modern Astronomy and Astrophysics (Nanjing University), Ministry of Education, People's Republic of China*

<sup>6</sup>*School of Physics and Electronic Engineering, Sichuan University of Science & Engineering, Zigong 643000, People's Republic of China*

### ABSTRACT

About 25% -50% of white dwarfs (WDs) are found to be polluted by heavy elements. It has been argued that the pollution could be caused by the tidal disruption of an approaching planet around the WD, during which a large number of clumps would be produced and would finally fall onto the WD. The reason that the planet approaches the WD is usually believed to be due to gravitational perturbations from another distant planet or stellar companion. However, the dynamics of the perturbation and the detailed partial disruption process are still poorly understood. In this study, we present an in-depth investigation of these issues. A triple system composed of a WD, an inner orbit planet, and an outer orbit planet is considered. The inner planet would be partially disrupted periodically in the long-term evolution. Fragments generated in the process are affected by the gravitational perturbations from the remnant planet, facilitating their falling toward the WD. The mass loss rate of the inner planet depends on both its internal structure and also on the orbital configuration of the planetary system.

*Keywords:* White dwarf stars (1799), Exoplanets (498), Dynamical evolution (421), Tidal disruption (1696)

### 1. INTRODUCTION

White dwarfs (WDs) are the final product of the evolution of most stars (90%) in the Universe, providing important information for understanding the formation and evolution of stars. During the evolution of WDs, heavy elements sink into the interior under strong gravity, while light elements float up to the surface so that there should be no heavy elements on the surface of the WDs (Paquette et al. 1986). However, about 25%–50% of observed WDs have strong emission or absorp-

tion lines of metals in their spectra, which points to the presence of metal pollution in their atmospheres (Zuckerman et al. 2003; Koester et al. 2014). The metal elements (Veras 2021; Klein et al. 2021; Budaj et al. 2022) that pollute the atmosphere of WDs may originate from disintegrated asteroids or planets (Debes & Sigurdsson 2002; Jura 2003; Antoniadou & Veras 2016; Veras & Wolszczan 2019; Duvvuri et al. 2020; Veras 2020). In a WD-asteroid/planet system, if the asteroid or planet enters the tidal disruption radius of the central object, it will be disintegrated under the action of tidal forces, forming a ring or disc (Veras et al. 2014; Malamud & Perets 2020a). The generated fragments could be accreted onto the surface of the WD under various interactions.

According to the theory of stellar evolution, the progenitor of a WD would significantly expand during the post-main sequence evolution stages and engulf any planets that previously existed within a few au ( $1.5 \times$

Corresponding author: Abdusattar Kurban  
akurban@xao.ac.cn

Corresponding author: Na Wang  
na.wang@xao.ac.cn

Corresponding author: Xia Zhou  
zhouxia@xao.ac.cn

$10^{13}$  cm) around the host star (Sato et al. 2008; Villaver & Livio 2009; Kunitomo et al. 2011). However, increasing evidence suggests that WDs could have close-in celestial companions, which include multiple fragments or asteroids (Granvik et al. 2016; Xu et al. 2016; Vanderbosch et al. 2021; Farihi et al. 2022), debris discs/rings (e.g., Koester et al. 2014; Farihi 2016), minor planets (Vanderburg et al. 2015; Manser et al. 2019; Blackman et al. 2021; Vanderbosch et al. 2020; Guidry et al. 2021), and even major planets (Thorsett et al. 1993; Luhman et al. 2011; Gänsicke et al. 2019; Vanderburg et al. 2020).

The origin of these close-in asteroids and planets is still highly uncertain, but intuitive speculation is that they might be the outcome of various dynamic processes. Firstly, scattering in a multi-planet system can form a close-in planet around the WD. Strong short-term gravitational interactions in the multi-planet system cause orbital instabilities, i.e., one planet may be perturbed by another planet with approximately equal or greater mass and would be eventually scattered toward the WD (Debes & Sigurdsson 2002; Bonsor et al. 2011; Debes et al. 2012; Veras et al. 2013; Frewen & Hansen 2014; Bonsor & Veras 2015; Veras et al. 2016, 2017, 2018; Mustill et al. 2018). The gravitational instability increases for a smaller planet mass, a larger orbital eccentricity, and the effect is enhanced when the number of planets increases in the system (Maldonado et al. 2020a,b, 2021; Veras 2021). Such gravitational instabilities in multi-planet systems increase metal pollution of WDs and can explain the observed fraction of polluted WDs (Li et al. 2021; Maldonado et al. 2022; Stock et al. 2022; O'Connor et al. 2022). Secondly, it has been argued that secular effects such as the Kozai-Lidov mechanism (Lidov 1962; Kozai 1962; Naoz 2016) might be a feasible approach to form close-in planets around WDs. The perturbation from a distant planet or stellar companion can push a planet to the tidal disruption region around the WD (Bonsor & Veras 2015; Hamers & Portegies Zwart 2016; Petrovich & Muñoz 2017; Muñoz & Petrovich 2020; Stephan et al. 2017, 2021). Thirdly, the capture of a free-floating planet by a WD (e.g., Kremer et al. 2019) or WD planetary system (e.g., Goulin-ski & Ribak 2018), or the exchange of a planet between the binary stars (e.g., Kratter & Perets 2012) can also form a close-in planetary system. The close-in planet WD J0914+1914 b is most likely the outcome of scattering (Gänsicke et al. 2019; Veras & Fuller 2020) or the Kozai-Lidov migration (Stephan et al. 2021), while the formation of WD 1856+534 b might be ascribed to the Kozai-Lidov effect (Muñoz & Petrovich 2020; O'Connor et al. 2021).

To understand the metal pollution in the atmosphere of WDs, it is necessary to study the accretion process of disintegrated fragments. Previously, the process has been investigated in context of various mechanisms such as the Poynting-Robertson drag effect (Rafikov 2011a; Veras et al. 2014, 2015b; Veras 2020), the collisional grind down (Jura 2003; Wyatt et al. 2007; Li et al. 2021; Brouwers et al. 2022), the Yarkovsky effect (Rafikov 2011a; Veras et al. 2014, 2015b; Veras 2020), the gravitational perturbation of a distant planet on fragments (Li et al. 2021), the action of previously existing matter (Malamud et al. 2021), the Alfvén wave drag caused by magnetic field (Hogg et al. 2021; Zhang et al. 2021), and sublimation (Veras et al. 2015a). Some authors (Li et al. 2021; Brouwers et al. 2022; Veras et al. 2022) have even considered the joint effect of multiple mechanisms mentioned above to analyze the dynamic process of debris accretion. In these works, the accretion timescale is usually longer than  $10^4$  yr and the accretion rate in the asteroid disruption scenario is typically smaller than  $10^{13}$  g s $^{-1}$ .

As previously mentioned, the processes such as scattering, capturing, and the Kozai-Lidov mechanism can lead to highly eccentric, close-in planetary systems. In these scenarios, the formation of a close-in orbit may occur gradually, depending on the configuration of the planetary system:

- The gradual approach occurs under the action of the Kozai-Lidov mechanism alone. For a planet in a stable three-body system where dynamical instability never occurs, the long-term Kozai-Lidov effect makes it possible that the planet's periastron distance gradually decreases.
- The gradual approach could occur under the combined effect of the short-term dynamical processes (scattering or capturing) and the long-term Kozai-Lidov effect. For the combination of scattering and the Kozai-Lidov effect, stable eccentric orbit configuration with periastron distance lying outside the partial disruption radius forms first due to the planet-planet scattering, then the planet in the inner orbit further evolves under the Kozai-Lidov perturbations from the outer giant planets (Nagasawa & Ida 2011) or binary companion (Mustill et al. 2022), causing a gradual decrease of the periastron distance. For the combination of capturing and Kozai-Lidov effect, stable eccentric orbit configuration forms via the capture of a planet by a WD-planet system (e.g., Goulin-ski & Ribak 2018; Kremer et al. 2019) first, then the Kozai-Lidov effect due to the outer planet further excites the ec-

centricity of the inner orbit planet in subsequent evolution process, which results in a gradual decrease in the periastron distance.

The planet may experience many partial disruptions during the long-term approaching process and the main portion of the planet could survive after each partial disruption. In this study, we investigate the accretion of tidal debris by the WD. The gravitational perturbation from the remnant planet on the accretion will be considered.

The structure of our paper is organized as follows. In Section 2, we describe the model used to analyze the orbit evolution of a triple system. In Section 3, the mass loss during the planet’s long-term orbit evolution will be calculated. The effects of gravitational perturbations from the remnant planet on the accretion of tidal fragments are studied in Section 4. The fate of the remnant planet and the actions of other forces that affect the tidal debris are discussed in Section 5. Finally, Section 6 presents our conclusions.

## 2. MODEL

The disruption of a planet in a multi-planet system can account for the WD pollution. In this case, the eccentricity of the inner orbit planet must be excited to an extreme value by the gravitational perturbations from the outer orbit objects. For simplicity, let us consider a planetary system composed of a central WD and two planets as illustrated in Figure 1. According to Kepler’s third law, the orbital period ( $P_{\text{orb}}$ ) and semi-major axis ( $a$ ) of a planet are related to each other as  $P_{\text{orb}}^2 = 4\pi^2 a^3 / [G(M_{\text{WD}} + m_{\text{pl}})]$ , where  $m_{\text{pl}}$  is the mass of the planet. The distance between the WD and the planet at phase  $\theta$  is  $r = a(1 - e^2)/(1 + e \cos \theta)$  for an eccentric orbit, where  $e$  is the orbital eccentricity. The argument and ascending node of the orbit are denoted as  $\omega$  and  $\Omega$ , respectively. We will use subscripts 1 and 2 to describe the parameters of the inner and outer orbit planets, respectively. The relative inclination angle between the two orbits is denoted as  $i$ .

### 2.1. Structural parameters of planets

Currently, the observed mass range of planets is very wide. It was speculated that the low-mass (super-Earth or Neptune-like) planets may be equally common in a wide range of orbits around the progenitors of WDs and contribute to some fraction of WD pollution (Veras et al. 2016; Mustill et al. 2018). Recently, rocky planets of masses  $\sim 40M_{\oplus}$  (TOI-849 b, Armstrong et al. 2020) and  $\sim 73M_{\oplus}$  (TOI-1853 b, Naponiello et al. 2023) have been observed, thought to be composed of a heavy element core and a thin hydrogen-helium atmosphere. The dy-

namical evolutionary properties of such low-mass planetary systems have been extensively investigated, paying special attention to the mass distribution function (Maldonado et al. 2020a,b). In this study, we will investigate similar planetary systems composed of such planets.

For simplicity, a two-layer (iron core and rocky mantle) rocky planet is assumed to be in the inner orbit. The main parameters (mass and radius) of the planet are calculated by using the equation of states (EOSs) widely used in exoplanet modeling, including iron (Fe) material considered in Smith et al. (2018) and rocky material ( $\text{MgSO}_3$ ) considered in Seager et al. (2007). Therefore, we take the parameter sets as  $m_{\text{pl},1} = 9.8M_{\oplus}$ ,  $20.7M_{\oplus}$ ,  $m_{\text{pl},2} = 9.55 \times 10^{-4}M_{\odot} (1M_{\text{Jup}})$ ,  $M_{\text{WD}} = 0.6M_{\odot}$ . Figure 2 shows the internal mass-radius profile for the two exemplar planets. Some key parameters (total mass  $m_{\text{pl},1}$  and radius  $R_{\text{pl},1}$ , iron core mass  $m_{\text{pl},1}^{\text{Fe}}$  and radius  $R_{\text{pl},1}^{\text{Fe}}$ , and iron mass fraction  $f_{\text{Fe}} = m_{\text{pl},1}^{\text{Fe}}/m_{\text{pl},1}$ ) are listed in Table 1.

**Table 1.** Key parameters of two exemplar planets considered in this study.

$m_{\text{pl},1}$ ( $M_{\oplus}$ )	$R_{\text{pl},1}$ (km)	$m_{\text{pl},1}^{\text{Fe}}$ ( $M_{\oplus}$ )	$R_{\text{pl},1}^{\text{Fe}}$ (km)	$f_{\text{Fe}}$ (%)
9.8	11634.8	4.6	6507.8	47
20.7	13800.4	10.5	7744.1	51

### 2.2. Orbital parameters of planets

The orbital parameters of the planets could be closely related to their origin. First, orbit configuration with  $0 \lesssim e \lesssim 1$  and  $a \gtrsim 1$  can form through the capture of a planet by a WD-planet system (e.g., Goulini & Ribak 2018). Second, the orbital parameters may be affected by the evolution history of the WD’s main sequence (MS) progenitor. For  $M_{\text{WD}} \sim 0.6M_{\odot}$ , the mass of its progenitor star should be  $M_{\text{MS}} \sim 1.5M_{\odot}$  according to Cummings et al. (2018). The envelope of such a star expands to about 0.8–2 au during the red giant branch (RGB) and asymptotic giant branch (AGB) stage (Mustill & Villaver 2012; Villaver et al. 2014; Veras 2016a; Veras & Fuller 2020). Low-mass planets initially resided inside the maximum stellar radius can still survive since their orbits will expand due to the mass loss of the progenitor during the giant branch phase (Mustill & Villaver 2012). For a planet in a near-circular orbit, the adiabatic stellar mass loss causes the orbit to expand by a magnitude of approximately  $M_{\text{MS}}/M_{\text{WD}} = 2.5$  and finally triggers dynamical instabilities, i.e. planetary systems that are stable in the MS stage become unstable at the onset of the WD stage (Debes & Sigurdsson 2002;

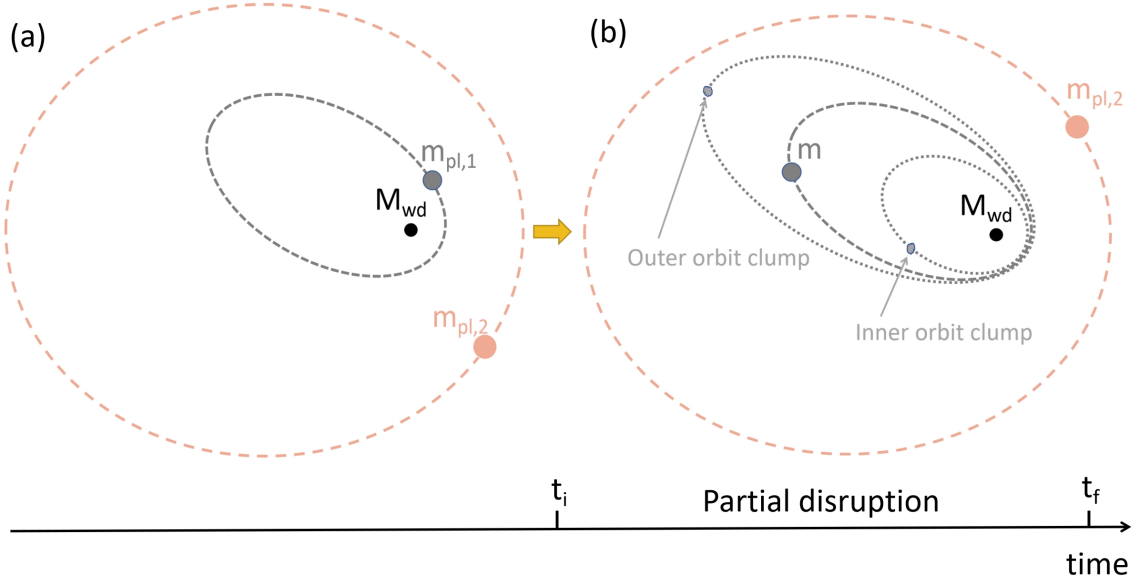


**Figure 1.** Schematic picture (not to scale) for the evolution of a triple system composed of a WD  $M_{\text{WD}}$ , a planet  $m_{\text{pl},1}$  in the inner orbit, and a planet  $m_{\text{pl},2}$  in the outer orbit. (a) Orbital evolution prior to partial tidal disruption, where  $m_{\text{pl},1}$  remains safe until its orbit evolves to the time point  $t_i$  at which the partial disruption starts. (b) Illustration of the partial disruption of the planet  $m_{\text{pl},1}$ , where  $m$  represents the remnant of  $m_{\text{pl},1}$  in each partial disruption that occurred during the time interval  $\Delta t = t_f - t_i$ , where  $t_f$  is the stopping time of partial disruption. The dotted ellipses represent the orbits of clumps in the inner and outer streams with respect to the orbit of  $m$ .

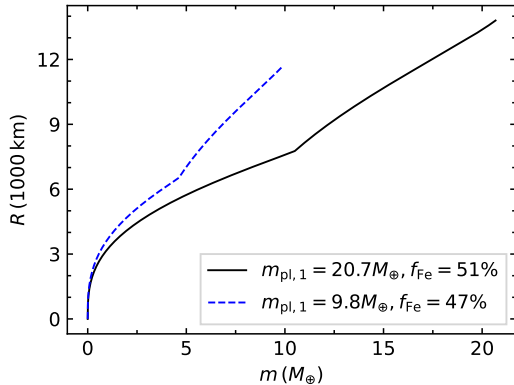


**Figure 2.** Internal mass and radius profile for a planet with  $m_{\text{pl},1} = 9.8M_{\oplus}$  (dashed line) or  $m_{\text{pl},1} = 20.7M_{\oplus}$  (solid line).

Mustill et al. 2014; Veras 2016b). During the unstable phase, ejection, collision, and scattering processes may occur till the separations between the remaining planets become wide enough so that the system be stabilized again (Adams & Laughlin 2003; Mustill et al. 2014, 2018; Frewen & Hansen 2014; Veras et al. 2016; Maldonado et al. 2020b, 2021, 2022). A planet with an initial semi-major axis of  $\sim 2$  au at the MS stage may expand to an orbit of  $\sim 5$  au due to mass loss of the progenitor. The planet could migrate inward to an orbit of  $\sim 2$  au again due to recurrent close scattering, which has been proved by numerical simulations for planetary

systems composed of equal-mass planets (Nagasawa & Ida 2011).

In short, orbital configurations with  $0 \lesssim e \lesssim 1$  and  $a \gtrsim 1$  are possible in realistic cases thanks to various dynamical interactions such as scattering and/or capturing at the WD stage. In this study, we take two different orbital configurations as: (A)  $a_1 = 3$  au,  $a_2 = 18$  au,  $e_1 = 0.8$ ,  $e_2 = 0.3$ ; (B)  $a_1 = 6$  au,  $a_2 = 44.1$  au,  $e_1 = 0.8$ ,  $e_2 = 0.3$ .

### 2.3. Orbital evolution

The dynamically stable configurations formed from planet-planet scattering or capturing in a WD-planet system will further evolve via the secular effect, the Kozai-Lidov mechanism. In this secular evolution process, the semi-major axis remains nearly constant while the eccentricity oscillates. We now assess the stability of the planetary system. The stability of triple systems has been studied for a long time (Eggleton & Kiseleva 1995; Mardling & Aarseth 2001). The stability condition can be expressed as (e.g., He & Petrovich 2018)

$$\frac{a_2(1-e_2)}{a_1} > 2.8 \left[ \left( 1 + \frac{m_{\text{pl},2}}{M_{\text{WD}} + m_{\text{pl},1}} \right) \frac{1+e_2}{(1-e_2)^{1/2}} \right]^{2/5} \times \left( 1 - \frac{0.3i}{180^\circ} \right). \quad (1)$$



The parameters of the planetary systems considered in our study (both Case A and Case B) satisfy this stability condition so that the triple systems are stable on long timescales. In the subsequent evolution, the orbital elements of the planet in the inner orbit (with mass  $m_{\text{pl},1}$ ) periodically change due to the perturbation from the planet in the outer orbit (with mass  $m_{\text{pl},2}$ ) via the Kozai-Lidov mechanism. Since  $m_{\text{pl},1} \ll M_{\text{WD}}$ , the inner orbit planet can be regarded as a test particle. To calculate the orbital evolution of the system, we use the secular code<sup>1</sup> developed by Bhaskar et al. (2021), which adopts the double-averaging method and can accurately describe the evolutionary properties of hierarchical and mildly hierarchical systems. We take 0.01% of the Kozai timescale  $t_k = \frac{M_{\text{WD}}}{m_{\text{pl},2}} (1 - e_2^2)^{3/2} \left(\frac{a_2}{a_1}\right)^3 P_{\text{orb},1}$  as the time step in our secular calculations (i.e.,  $10^{-4} t_k$ ). The secular results are compared with the standard  $N$ -body simulation results acquired by using the package MERCURY (Chambers 1999). The Bulirsch-Stoer integration algorithm with a time step of 5% of the period of the inner orbit planet (i.e.,  $0.05 P_{\text{orb},1}$ ) and a tolerance parameter of  $10^{-12}$  are used for  $N$ -body simulations. As shown in Figure 3, the secular results consist well with the  $N$ -body simulation results. It can be seen that the periastron distance ( $r_{\text{p},1} = a_1(1 - e_1)$ ) of the inner orbit planet decreases periodically to a small value so that it could be partially disrupted at the periastron.

### 3. EVOLUTION OF THE INNER ORBIT PLANET

The periodic change of the periastron distance leads to a continuous decrease of the mass of the inner orbit planet since it would be partially disrupted every time it passes through the periastron. The mass of the surviving portion can be evaluated by considering the  $r_{\text{p},1}$  parameter and the partial disruption criteria.

#### 3.1. Tidal disruption of a planet

If a planet is located too close to its host WD, it will be tidally disrupted since the host's tidal force is larger than the planet's self-gravity at its surface (Hills 1975; Rees 1988). For a gravity-dominated planet, the characteristic tidal disruption radius can be estimated as

$$r_{\text{td}} = R \left( \frac{2M_{\text{WD}}}{m} \right)^{1/3}, \quad (2)$$

where  $m$  and  $R$  are the mass and radius of the planet, respectively. When the separation between the planet and the central WD ( $r$ ) is smaller than  $r_{\text{td}}$ , it would be completely disrupted. But in the more general cases that  $r$  is

slightly larger than  $r_{\text{td}}$ , a partial disruption will occur. It has been shown that the partial disruption occurs as long as  $r < 2.7 r_{\text{td}}$  (Guillochon et al. 2011; Liu et al. 2013). Such a process has also been explored through numerical simulations (e.g., Guillochon & Ramirez-Ruiz 2013; Malamud & Perets 2020a; Ryu et al. 2020; Law-Smith et al. 2020; Coughlin & Nixon 2022). Astrophysical phenomena possibly connected with partial disruption have also been reported (Manser et al. 2019). The properties of tidal interaction between a planet and a compact star (neutron star or strange quark star) have also been investigated for different scientific purposes such as searching for strange quark matter planets (Geng et al. 2015; Huang & Yu 2017; Kuerban et al. 2019, 2020), fast radio bursts (Kurban et al. 2022) and repeating X-ray bursts (Kurban et al. 2024).

For the highly elliptical orbit considered in this study,  $r$  is phase-dependent and varies in a very wide range. The planet is affected by the tidal effect mainly near the periastron,  $r_{\text{p},1} = a_1(1 - e_1)$ , and it is relatively safe at other orbital phases. When the partial disruption condition is satisfied, i.e.  $r_{\text{td}} < r < 2.7 r_{\text{td}}$ , the surface material of the planet will be stripped off but the underneath portion will retain its integrity. In our cases, the inner orbit planet will be subject to partial disruption when its periastron distance decreases to  $r_{\text{p},1} = 2.7 r_{\text{td}}$  during the orbit evolution process. For example, the dashed and solid horizontal lines in Figure 3 represent the partial disruption distances for  $m_{\text{pl},1} = 9.8 M_{\oplus}$  and  $m_{\text{pl},1} = 20.7 M_{\oplus}$ , respectively. The dashed and solid vertical lines denote the corresponding starting ( $t_i$ ) and stopping ( $t_f$ ) time of partial disruption. It can be seen that for planets with different masses, the partial disruption process stops at different  $t_f$  in Case A, while it stops at the same  $t_f$  in Case B.

#### 3.2. Mass loss

During the partial disruption process, the total mass loss from the Lagrangian points  $L_1$  and  $L_2$  in an encounter is  $\Delta m = \Delta m_1 + \Delta m_2$ , where  $\Delta m_1$  and  $\Delta m_2$  are the mass loss from the  $L_1$  and  $L_2$ , respectively. Usually, the mass loss is asymmetric, and approximately 75% of  $\Delta m$  is stripped from  $L_1$  (Faber et al. 2005), i.e.  $\Delta m_1 \approx 0.75 \Delta m > \Delta m_2$ . In our cases,  $\Delta m$  depends on both the periastron separation and the planet's structure, which vary with time. As mentioned earlier, we have  $r_{\text{p},1} = r_{\text{td}}/\beta$  for the partial disruption condition, where  $\beta = 1/2.7$ . Then the mass evolution of the surviving portion of the planet can be expressed as

$$\frac{dm}{dt} = \frac{3r_{\text{p},1}^2 \beta^3}{2M_{\text{WD}}} \left( \frac{3R^2}{m} \frac{dR}{dm} - \frac{R^3}{m^2} \right)^{-1} \frac{dr_{\text{p},1}}{dt}, \quad (3)$$

<sup>1</sup> The code can be downloaded at <https://github.com/bhareeshg/gda3bd>

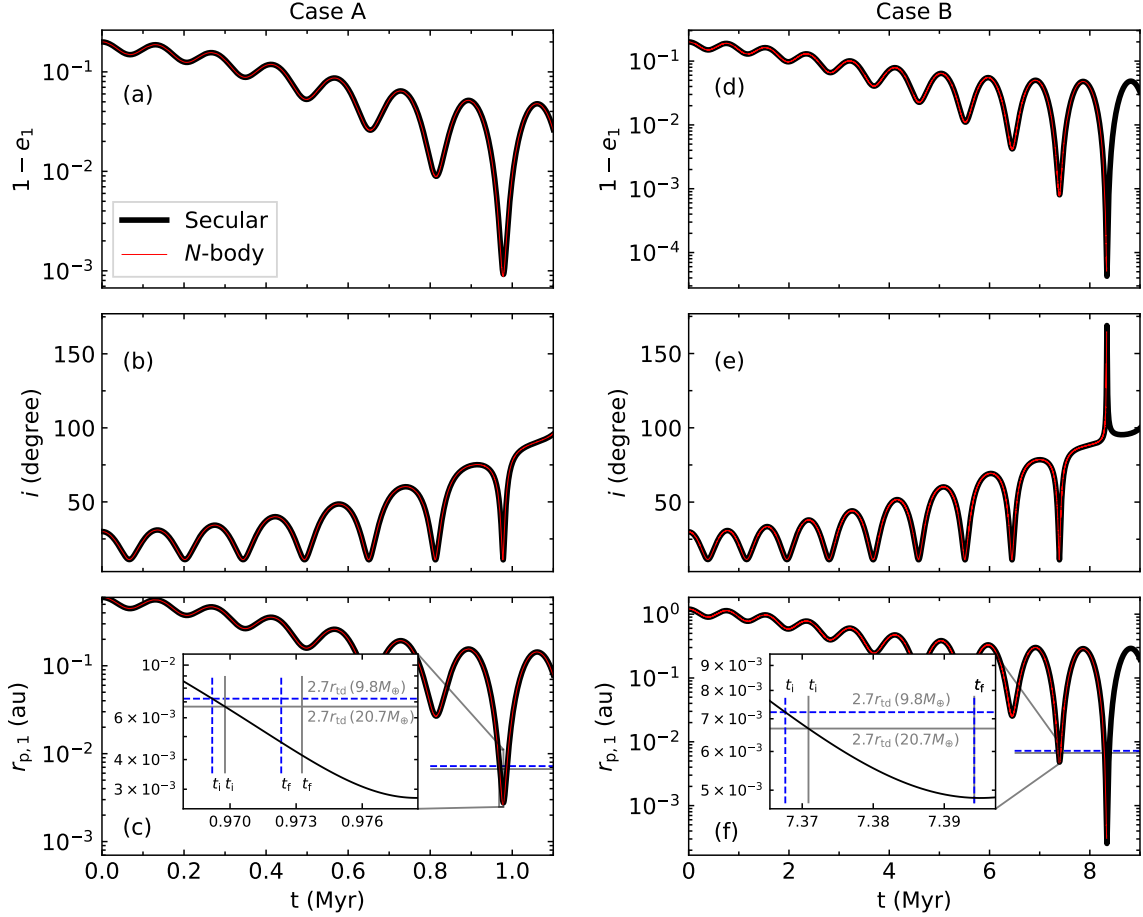


**Figure 3.** Evolution of the eccentricity (Panels a and d), inclination (Panels b and e), and periastron distance (Panels c and f) for the inner orbit planet (test particle) in a triple system. The mass of the central WD is taken as  $M_{\text{WD}} = 0.6M_{\odot}$  and the outer orbit planet has a mass of  $m_{\text{pl},2} = 9.55 \times 10^{-4}M_{\odot} (1M_{\text{Jup}})$ . The initial values of the argument, ascending node, and relative inclination of the two orbits are taken as  $\omega_1 = 180^\circ$ ,  $\omega_2 = 0^\circ$ ,  $\Omega_1 = 0^\circ$ ,  $\Omega_2 = 0^\circ$ , and  $i = 30^\circ$ . Two cases are considered for the initial values of the semi-major axis and eccentricity. Case A (left panels):  $a_1 = 3$  au,  $a_2 = 18$  au,  $e_1 = 0.8$ ,  $e_2 = 0.3$ . Case B (right panels):  $a_1 = 6$  au,  $a_2 = 44.1$  au,  $e_1 = 0.8$ ,  $e_2 = 0.3$ . In each panel, the black and red lines show the results of the secular and  $N$ -body simulations, respectively. But note that they are almost overlapped since the results are very close to each other. The dashed and solid horizontal lines represent the expected partial disruption distances for  $m_{\text{pl},1} = 9.8M_{\oplus}$  and  $m_{\text{pl},1} = 20.7M_{\oplus}$ , respectively. The dashed and solid vertical lines denote the corresponding starting ( $t_i$ ) and stopping ( $t_f$ ) time of partial disruption. In Case B,  $t_f$  is essentially the same for different masses.

where  $dr_{\text{p},1}/dt$  is the varying rate of planet's periastron distance.

Taking the planet mass as  $m_{\text{pl},1} = 9.8M_{\oplus}$  or  $20.7M_{\oplus}$ , we have solved the above equation numerically to determine the mass loss of the inner orbit planet for the cases of A and B. Here, we use  $\Delta t$  to denote the period that the planet's periastron distance  $r_{\text{p},1}$  changes from  $r_{\text{p},1}(t_i)$  to  $r_{\text{p},1}(t_f)$ . It corresponds to the time interval between the starting ( $t_i$ ) and stopping ( $t_f$ ) time of the partial disruption process,  $\Delta t = t_f - t_i$ . The initial values of mass and periastron are taken as  $m_0 = m(t_i) = m_{\text{pl},1}$  and  $r_{\text{p},1}^0 = r_{\text{p},1}(t_i) = r_{\text{td}}(m_0)/\beta$ . Note that the material configuration inside the planet does not change dramatically after a partial disruption due to the tensile strength

and internal viscosity (e.g., Veras et al. 2019). The total number of orbital periods within the time interval  $\Delta t$  is  $N = \Delta t/P_{\text{orb},1}$ .

Figures 4 and 5 show our numerical results corresponding to cases A and B, respectively, which illustrate the evolution of the planet structure due to the mass loss during the close approach. It can be seen from the Figures that the surviving portion of the planet becomes smaller and smaller over a timescale of thousands of years, resulting in an increase in the mean density. Consequently, the percentage of the planet's iron composition increases at the final stages. Note that there is a large difference in the mass loss between Case A and Case B. This is mainly caused by the different orbit

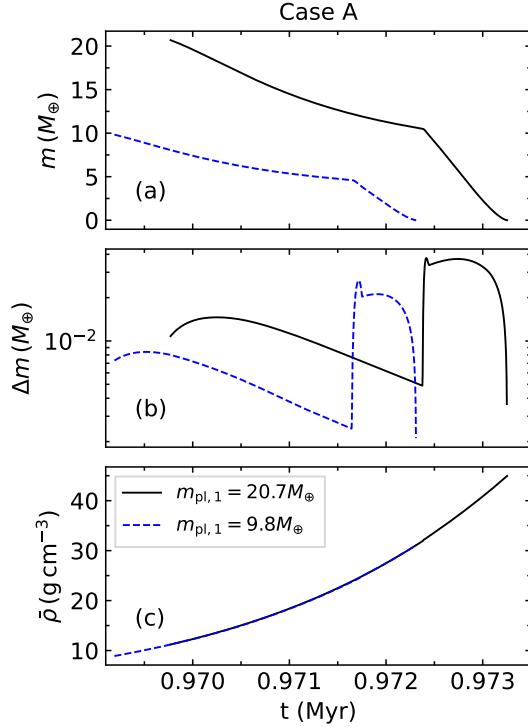


**Figure 4.** Evolution of the inner orbit planet during the partial disruption process for Case A: (a) Mass of the surviving portion, (b) mass loss, and (c) mean density. The dashed and solid lines correspond to the different initial masses of the planet,  $9.8M_\oplus$  and  $20.7M_\oplus$ , respectively.

evolution and different planetary structures. The two planets in Case A will experience complete disruption at different  $t_f$ . However, the remnant core survives in Case B and the partial disruption stops at the same  $t_f$  for the two objects. Note that the upward jumps in the mass loss curves are caused by the change of  $dR/dm$  at the core-mantel boundary. The planet with  $m_{pl,1} = 20.7M_\oplus$  in Case B keeps a fraction of its mantel so that its mass loss curve is different from others.

**Table 2.** Key parameters derived for the two cases of orbit configurations.

Orbit conf.	$m(t_i)$ ( $M_\oplus$ )	$m(t_f)$ ( $M_\oplus$ )	$\Delta t$ (yr)	$N$ (Orbit)	$\Delta M$ ( $M_\oplus$ )
Case A	9.8	0	3122	465	9.8
	20.7	0	3481	519	20.7
Case B	9.8	1.2	26600	1401	8.6
	20.7	11.1	23341	1229	9.6

From these calculations, we see that partial disruptions could occur repeatedly during the long-term evolution of the planet’s orbit. The total mass loss ( $\Delta M$ ),

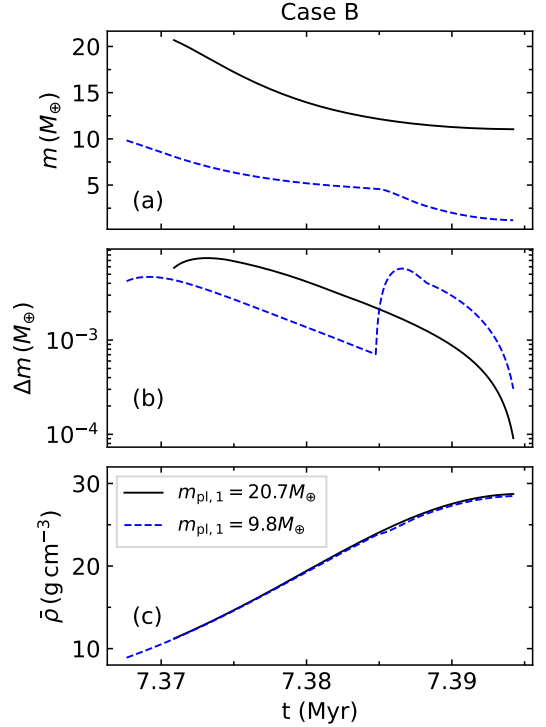


**Figure 5.** Same as in Figure 4 but for Case B.

which is defined as the change of the planet mass during the time interval  $\Delta t$ , can be calculated as  $\Delta M = m(t_i) - m(t_f)$ , where  $m(t_i) = m_{pl,1}$  is the initial mass and  $m(t_f)$  is the final mass after  $\Delta t$ . Table 2 presents our numerical results for these parameters. In Case A, we have  $\Delta t = 3122$  yr ( $N = 465$ ) and  $\Delta M = 9.8M_\oplus$  for  $m_{pl,1} = 9.8M_\oplus$ , while  $\Delta t = 3481$  yr ( $N = 519$ ) and  $\Delta M = 20.7M_\oplus$  for  $m_{pl,1} = 20.7M_\oplus$ . In Case B, we have  $\Delta t = 26600$  yr ( $N = 1401$ ) and  $\Delta M = 8.6M_\oplus$  for  $m_{pl,1} = 9.8M_\oplus$ , while  $\Delta t = 23341$  yr ( $N = 1229$ ) and  $\Delta M = 9.6M_\oplus$  for  $m_{pl,1} = 20.7M_\oplus$ . It shows that: (i) the planet will become an iron-rich or pure iron object via mass loss, and (ii) the mass loss process depends on the structure of the planet and the orbital configuration of the planetary system.

#### 4. ACCRETION OF CLUMPS

Numerical simulations on the tidal disruption of a planet around a WD (Malamud & Perets 2020a,b) show that the size of the generated clumps range from a few kilometers to hundreds of kilometers. The fate of the clumps produced during a partial disruption is different from that produced in a full disruption. A full disruption usually occurs in the cases of deep encounters which would lead to the formation of a ring/disc so that the generated clumps evolve mainly under the influence of non-gravitational effects (Veras et al. 2014, 2015b; Hogg

et al. 2021; Zhang et al. 2021). However, the clumps produced during a partial disruption process are affected by the gravitational perturbation from the remnant planet. They could be further tidally disrupted when they move closer to the WD. Note that these small bodies are generally dominated by intrinsic material strength but not gravity. As a result, the breakup separation is  $\sim 10^9$  cm for them (e.g., Zhang et al. 2021; Kurban et al. 2023). In this section, we will investigate the evolutionary tracks of these clumps.

#### 4.1. Orbital parameters of the clumps

In our framework, the orbit of the inner planet evolves with time. Here, we analyze the distribution of the orbits of the clumps generated during the partial disruption process. The semi-major axis of the clumps can be calculated by following Malamud & Perets (2020a),

$$a_{\text{cl}} = \begin{cases} a_1 \left(1 + a_1 \frac{2R}{d(d-R)}\right)^{-1}, & \text{(inner)} \\ a_1 \left(1 - a_1 \frac{2R}{d(d+R)}\right)^{-1}, & \text{(outer)} \end{cases} \quad (4)$$

where  $a_1$  is still the inner orbit planet’s original semi-major axis,  $d$  is the distance between the WD and the planet at the moment of break up (i.e.,  $d = r_{\text{p},1} = r_{\text{td}}(m)/\beta$ , with  $m$  being the mass of the remnant planet that evolves with time),  $R$  is the displacement of the clump relative to the planet’s mass center at the moment of breakup. Actually,  $R$  is the radius of the remnant planet here ( $R = 0$  corresponds to the planet’s center). In the above equation, “inner” means the clumps originate from the inner side of the planet, while “outer” means they come from the outer side. The clumps in the inner stream are all bound to the WD. For clumps originating from the planet’s face opposite to the WD, there is a critical displacement of  $R_{\text{crit}} = d^2/(2a_1 - d)$ . The clumps with  $R > R_{\text{crit}}$  are unbound while particles with  $R < R_{\text{crit}}$  are still bound to the WD (Malamud & Perets 2020a). We have checked the properties of the clumps in the outer stream (see Figure 1) and found that their orbits are bound to the WD when they are newly born from the remnant planet. But their orbits could be altered by the planet after a few orbits and may be scattered away finally. We will discuss this point in the next sections.

Combining Equation (4) and Kepler’s third law, we can obtain the orbital period of the clumps as

$$P_{\text{orb}}^{\text{cl}} = \left( \frac{4a_{\text{cl}}^3 \pi^2}{G(M_{\text{WD}} + m_{\text{cl}})} \right)^{1/2}. \quad (5)$$

After the disruption, the clumps return to the periastron ( $r_{\text{pl},1}$ ) at a time of  $t_{\text{re}} = P_{\text{orb}}^{\text{cl}}$ . Since  $r_{\text{p},1} = a_{\text{cl}}(1 - e_{\text{cl}}) \pm$

$R$ , the eccentricity of the clumps can be expressed as

$$e_{\text{cl}} = \begin{cases} 1 - \frac{r_{\text{pl},1} - R}{a_{\text{cl}}}, & \text{(inner)} \\ 1 - \frac{r_{\text{pl},1} + R}{a_{\text{cl}}}, & \text{(outer)} \end{cases} \quad (6)$$

#### 4.2. Fate of the clumps

Clumps in the outer orbit are affected by the perturbation from both the remnant planet and the outer orbit planet (whose mass is  $m_{\text{pl},2}$ ). Their evolution is very complicated. They could be ejected from the system or could have chaotic behavior. Generally, it is hard to describe their properties in a simple way. Here, we mainly concentrate on the inner orbit clumps in this study.

After the birth of the clumps, the WD, clumps, and the surviving portion of the planet form a multi-body system, in which the gravitational interactions among various objects are very complicated. For simplicity, we omit the interactions between the clumps. To follow the evolution of a particular clump, we can take the clump, the WD, and the surviving part of the planet as a triple system. The stability of such a triple system can be accessed by using Equation (1). It is found that the configuration does not satisfy the stability condition. In fact, we have  $a_1(1 - e_1)/a_{\text{cl}} < 0.2$ , which is well below the stability limit. It means that the secular interaction (Kozai-Lidov mechanism) will be broken down, i.e., Kozai-Lidov mechanism can not accurately describe clump’s orbit evolution (e.g., Perets & Kratter 2012; Naoz et al. 2011; Katz & Dong 2012; Antonini & Perets 2012; Bode & Wegg 2014). In such a case, strong perturbation from the remnant planet (e.g., Toonen et al. 2022) will lead to a large orbital eccentricity for the clump so that it will lose its angular momentum on a relatively short timescale (e.g., Antonini et al. 2014, 2016; Hamers et al. 2022; Kurban et al. 2023). Below, we present a detailed estimation on this point.

The clump returns to the periastron in a time of  $t_{\text{re}} = P_{\text{orb}}^{\text{cl}}$  after the disruption (Malamud & Perets 2020a; Zanazzi & Ogilvie 2020; Rossi et al. 2021). Its specific angular momentum is  $j_{\text{cl}} = \sqrt{1 - e_{\text{cl}}^2}$ , which is small compared with that of the planet. Perturbation from the remnant planet leads to a quick loss of the clump’s angular momentum. The angular momentum changes from  $j_{\text{cl}}$  to almost zero on a timescale of the order of the inner orbit period, causing the clump to effectively fall onto the WD (e.g., Antonini et al. 2014; Kurban et al. 2023). It indicates that the periastron of the clump jumps to a very small value, which is mainly caused by the energy exchange between the clump and the remnant planet due to their gravitational interactions (e.g., Zhang et al. 2023). The evolution timescale of the angular momentum of the clump ( $t_{\text{evo}}$ ) can be



expressed as (e.g., Antonini et al. 2014)

$$\left[ \frac{1}{j_{\text{cl}}} \frac{dj_{\text{cl}}}{dt} \right]^{-1} \approx \frac{P_{\text{orb}}^{\text{cl}}}{5\pi} \frac{M_{\text{WD}}}{m} \left[ \frac{a_1(1-e_1)}{a_{\text{cl}}} \right]^3 \sqrt{1-e_{\text{cl}}}. \quad (7)$$

Adopting the parameters used in Figures 4 and 5, we have estimated the orbital periods and the evolution timescales of the clumps' angular momentum. Table 3 lists the results at the time of  $t_i$  and  $t_c$  in Case A, where  $t_c$  is the critical time at which  $m \approx 0.5M_{\oplus}$  and  $t_{\text{evo}} < P_{\text{orb}}^{\text{cl}} < P_{\text{orb}}$  for  $t \lesssim t_c$ . For Case B, the results at the time of  $t_i$  and  $t_f$  are listed in Table 4. It can be seen that  $t_{\text{evo}} < P_{\text{orb}}^{\text{cl}} < P_{\text{orb}}$  for  $t \lesssim t_f$ . Since the clumps lose their angular momentum in a time of  $t_{\text{evo}}$  after the second orbit (i.e., the second periastron passage), the clump's total travel time from their birth at the planet to the WD will be  $t_{\text{trav}} \lesssim 3P_{\text{orb}}^{\text{cl}}$  (Kurban et al. 2023). It means that the clump could fall onto the WD in a short time.

#### 4.3. Accretion rate

The clumps would fall onto the WD on a timescale shorter than a few  $P_{\text{orb}}$  after their birth. It means that the lost mass of the planet during an encounter,  $\Delta m_1$ , would be accreted by the WD in this period. We thus can simply estimate the accretion rate. Figure 6 shows the long-term evolution of the accretion rate ( $\dot{m} = 0.75dm/dt$ ) for our cases A and B. We see that the accretion rate is  $\dot{m} \sim 10^{17}\text{--}10^{18} \text{ g s}^{-1}$  in Case A and  $\dot{m} \sim 10^{15}\text{--}10^{17} \text{ g s}^{-1}$  in Case B. It depends on the planet's structure and the periastron distance of the orbit. In both cases, the accretion rate changes in a complex way because  $dr_{\text{p},1}/dt$  and  $dR/dm$  vary in the process.

The total mass loss is  $\Delta M = \Delta M_1 + \Delta M_2$ , where  $\Delta M_1$  is the sum of the mass lost from  $L_1$  and  $\Delta M_2$  is the sum of the masses lost from  $L_2$ , respectively. The average accretion rate can be simply calculated as  $\langle \dot{M} \rangle = \Delta M_1/\Delta t \approx 0.75\Delta M/\Delta t$  (here  $\Delta t = t_c - t_i$  and  $\Delta M = m(t_i) - m(t_c)$  for Case A). The characteristic accretion rate for cases A and B are presented in Table 3 and 4, respectively. In Case A,  $\langle \dot{M} \rangle \approx 4.4 \times 10^{17} \text{ g s}^{-1}$  for  $m_{\text{pl},1} = 9.8M_{\oplus}$ , and  $\langle \dot{M} \rangle \approx 8.5 \times 10^{17} \text{ g s}^{-1}$  for  $m_{\text{pl},1} = 20.7M_{\oplus}$ . In Case B,  $\langle \dot{M} \rangle \approx 4.6 \times 10^{16} \text{ g s}^{-1}$  for  $m_{\text{pl},1} = 9.8M_{\oplus}$ , and  $\langle \dot{M} \rangle \approx 5.9 \times 10^{16} \text{ g s}^{-1}$  for  $m_{\text{pl},1} = 20.7M_{\oplus}$ . When the planet mass is equal, the accretion rate in Case A is generally higher than that in Case B. The reason is that the decrease of  $r_{\text{p},1}$  in Case A is quicker than that in Case B during the partial disruption phases. The results show that the accretion rate is also governed by the planet's structure and orbital configuration, which is similar to the mass loss.

## 5. DISCUSSION

Depending on the planetary architecture, there are three possibilities for the final fate of the planet subjected to a long-term partial disruption process due to the orbital evolution caused by the Kozai-Lidov mechanism. Firstly, the planet could be destroyed completely before  $t_f$ , which may lead to the formation of a relatively massive remnant disc. Secondly, the main portion of the planet survives after a large number of partial disruptions during  $\Delta t$ . After  $t_f$  it could be further disrupted if  $r_{\text{p},1}$  still meets the partial disruption condition during the next high eccentricity phase of the Kozai-Lidov cycle, as in Case B. Thirdly, for some particular configurations, the remnant planet survives at  $t_f$  and acquires its maximum eccentricity ( $e_{\text{max}}$ ) at this point. In subsequent evolution, the eccentricity  $e$  remains less than  $e_{\text{max}}$ . Consequently, the partial disruption distance of the remnant planet will always be less than its periastron distance for  $t > t_f$  so that the tidal disruption process will no longer occur later. Our model extends the timescale across which a planet can be disrupted compared to a complete instantaneous tidal disruption at the Roche radius. Here we present some further analyses of the process.

#### 5.1. Iron-rich planetary remnant

In the multiple partial disruption process, the planet's mass gradually decreases together with the decrease of the periastron distance. The surface layer of the planet is stripped off at each periastron passage so that the percentage of iron composition in the remnant planet becomes higher and higher. The iron core may be surrounded by a layer of debris at the late stages of the partial disruption process. Such iron-rich objects have been discovered in recent years. For example, the minor planet SDSS J1228+1040 b was found to be embedded in a debris disc. The planet is about 0.003 au from its host star, well within the Roche radius of rubble-pile. However, it does not show any signatures of being disrupted now, implying that the object is actually an iron-rich planetary core with tensile strength and internal viscosity (Veras & Wolszczan 2019; Manser et al. 2019; O'Connor & Lai 2020).

Iron-rich planetary objects have also been discovered around other type of stars. For example, the terrestrial exoplanet GJ 367 b is found to be orbiting around an M-type star (Lam et al. 2021; Goffo et al. 2023). It has a mass of  $0.633M_{\oplus}$ , a radius of  $0.699R_{\oplus}$ , and a mean density of  $\bar{\rho} = 10.22 \text{ g cm}^{-3}$ , implying that its iron composition is about 90%. Its distance from the host star is 0.00709 au, which is well within the rubble-pile Roche radius. Interestingly, GJ 367 has two additional planets, GJ 367 c ( $> 4.13M_{\oplus}$ ) and GJ 367 d ( $> 6.03M_{\oplus}$ ), resid-

**Table 3.** Case A: the orbital period and angular momentum loss time for the clumps generated at time  $t_i$  and  $t_c$ , and the characteristic accretion rate during the time interval  $\Delta t = t_c - t_i$ .

$m(t_i)$ ( $M_\oplus$ )	$R(t_i)$ (km)	$P_{\text{orb}}^{\text{cl}}$ (day)	$t_{\text{evo}}$ (day)	$m(t_c)$ ( $M_\oplus$ )	$R(t_c)$ (km)	$P_{\text{orb}}^{\text{cl}}$ (day)	$t_{\text{evo}}$ (day)	$\langle \dot{M} \rangle$ ( $\text{g s}^{-1}$ )
9.8	11634.8	76.9	0.2	0.5	2894.4	167.2	0.4	4.4e+17
20.7	13800.4	49.1	0.1	0.5	2558.4	141.6	0.3	8.5e+17

**Table 4.** Case B: the orbital period and angular momentum loss time for the clumps generated at time  $t_i$  and  $t_f$ , and the characteristic accretion rate during the time interval  $\Delta t = t_f - t_i$ .

$m(t_i)$ ( $M_\oplus$ )	$R(t_i)$ (km)	$P_{\text{orb}}^{\text{cl}}$ (day)	$t_{\text{evo}}$ (day)	$m(t_f)$ ( $M_\oplus$ )	$R(t_f)$ (km)	$P_{\text{orb}}^{\text{cl}}$ (day)	$t_{\text{evo}}$ (day)	$\langle \dot{M} \rangle$ ( $\text{g s}^{-1}$ )
9.8	11634.8	83.1	0.2	1.2	3909.8	130.4	0.2	4.6e+16
20.7	13800.4	51.9	0.1	11.1	8183.3	44.8	0.1	5.9e+16

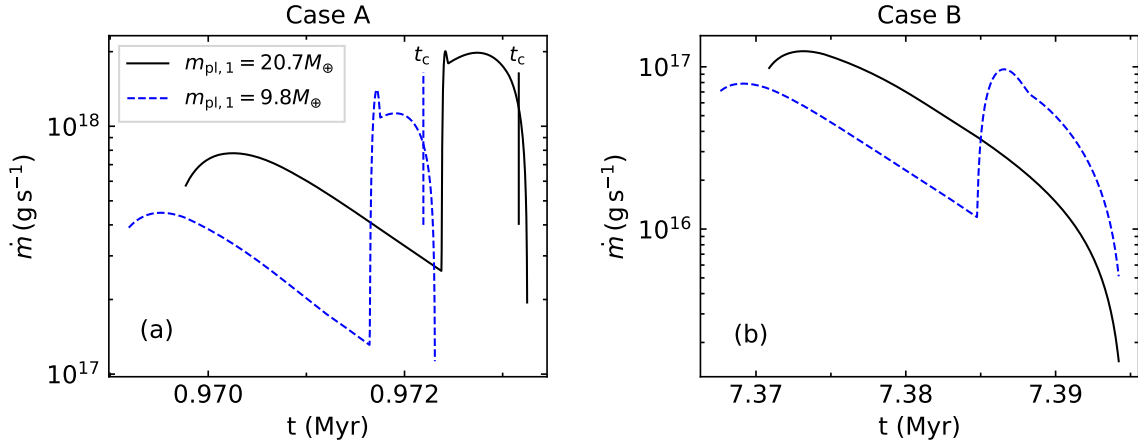


**Figure 6.** Accretion rate as a function of time for Case A (Panel a) and Case B (Panel b). In each panel, the dashed and solid line correspond to  $m_{\text{pl},1} = 9.8M_\oplus$  and  $m_{\text{pl},1} = 20.7M_\oplus$ , respectively. In Panel (a), the vertical lines marked with  $t_c$  represent the critical time at which  $m \approx 0.5M_\oplus$ .

ing outside the GJ 367 b (Goffo et al. 2023). Another exoplanet K2-141 b, which orbits around a K-type star, has a mass of  $4.97M_\oplus$ , a radius of  $1.51R_\oplus$ , and a mean density of  $\bar{\rho} = 7.96 \text{ g cm}^{-3}$ . It is 0.00747 au from its host star, which is also well within the rubble-pile Roche radius (Malavolta et al. 2018). K2-141 has another additional planet, K2-141 c (mass:  $7.41M_\oplus$ ), which also resides outside K2-141 b (Malavolta et al. 2018). The formation history of the iron-rich inner orbit planets in the above two planetary systems (GJ 367 and K2-141) is still not clear at present. A likely interpretation is that they may have experienced the same evolutionary history as in our framework.

### 5.2. Total accreted mass

The masses of the bodies that pollute WDs can be inferred from observations. For example, accumulated metal mass in the convective zone can be estimated by using the spectral features and WD atmospheric models

(Koester 2009). Girven et al. (2012) derived the lower limit of the total accreted mass of metals deposited in the convective zone as  $\sim 10^{16} - 10^{22} \text{ kg}$  for DBZ WDs. Harrison et al. (2021) also argued that DZ WDs systems in which the accretion process has come to an end can be unique probes for estimating the mass of the polluting body. They found that the mass of the pollutant body is generally consistent with that of large asteroids and/or the Moon.

However, since the tidal disruption, accretion, and sinking of accreted materials is a complicated process, the mass of metals in the convective zone is not necessarily equivalent to the mass of the polluting body in some cases. Firstly, a fraction of the planet's mass may escape from the system after the tidal disruption. In the complete tidal disruption cases, some materials could be unbounded and would be ejected (Malamud & Perets 2020a,b). In the partial disruption cases, mate-

rials in the outer bound stream may also be scattered away from the system due to perturbation from the remnant planet (Kurban et al. 2023, 2024). Secondly, some of the energy released during the accretion process will be thermalized and emitted in the form of X-rays (Cunningham et al. 2022; Estrada-Dorado et al. 2023), which may more or less lead to an extra mass loss. Thirdly, some of the accreted mass may sink too quickly and be deposited much deeper than the upper convective zone so that they are no longer observable. In fact, metals heavier than carbon will pass through the convection zone quickly, on a timescale ranging from days to weeks for DA WDs, or in a few Myr for DB WDs (Wyatt et al. 2014). This will cause an underestimation of the total accreted mass based on observations involving only the convective zone. Finally, some of the mass may be left in a remnant accretion disc. For example, the accretion lasts for a long period in most of DA WDs (Kleinman et al. 2013; Veras 2016b; Hollands et al. 2018; Blouin & Xu 2022), implying that large planets should be involved in the disruption process (Hamers & Portegies Zwart 2016; Petrovich & Muñoz 2017).

### 5.3. Accretion rate confronted with observations

The accretion rate inferred from the observed photospheric element abundances of DAZ WDs typically ranges from  $\sim 10^5 \text{ g s}^{-1}$  to  $\sim 10^8 \text{ g s}^{-1}$  (Koester et al. 2014). A high rate up to  $\sim 10^{11} \text{ g s}^{-1}$  is observationally inferred for a number of DBZ WDs (Farihi et al. 2012; Girven et al. 2012; Farihi 2016). The accretion rate derived from the X-ray observations of WD G 29-38 is approximately  $2 \times 10^9 \text{ g s}^{-1}$  (*Chandra* observation; Cunningham et al. 2022) or  $4.01 \times 10^9 \text{ g s}^{-1}$  (*XMM-Newton* observation; Estrada-Dorado et al. 2023). An instantaneous high accretion rate of  $1.45 \times 10^{14} \text{ g s}^{-1}$  was also derived from the X-ray luminosity of KDP 0005+5106 (Chu et al. 2021). When energy supply is assumed to come only from accretion, heating of the Ca II emission line region requires an accretion rate of  $10^{17}$ – $10^{18} \text{ g s}^{-1}$  (Hartmann et al. 2011). Note that this accretion rate can be lowered when considering the heating by energy dissipation through disc asymmetries or by absorbing photons from the WD (Hartmann et al. 2011).

Several models have been developed to explain the above observations. The Poynting-Robertson drag and/or the Yarkovsky effect can account for an accretion rate up to  $\sim 10^8 \text{ g s}^{-1}$  (Rafikov 2011a). Considering the additional viscosity of gas produced from sublimation would further increase the accretion rate, potentially leading to a runaway process with a peak rate of  $10^{10}$ – $10^{11} \text{ g s}^{-1}$  (Rafikov 2011b; Metzger et al. 2012). On the other hand, if the collisional grind-down

is taken into account, the peak accretion rate is found to vary from  $\sim 10^8 \text{ g s}^{-1}$  for a 50 km asteroid to  $\sim 10^{13} \text{ g s}^{-1}$  for a 500 km asteroid (Brouwers et al. 2022). It was also argued that an accretion rate of  $\sim 10^{10} \text{ g s}^{-1}$  could be attained due to the Alfvén-wave drag (Zhang et al. 2021). The high accretion rate associated with star-planet interaction can lead to bright X-ray emissions (Farihi et al. 2012; Girven et al. 2012). The accretion rate of  $1.45 \times 10^{14} \text{ g s}^{-1}$  inferred in KDP 0005+5106 strongly indicates the interaction of the WD with a Jupiter-like planet (Chu et al. 2021), which is still two orders of magnitude smaller than the lower limit of WDs accreting from stellar companions at a rate of  $\gtrsim 10^{16} \text{ g s}^{-1}$  (Mukai 2017). As delineated in Section 4.3, partial disruption of a planet can engender such high accretion rates. The accretion rate of  $10^{17}$ – $10^{18} \text{ g s}^{-1}$  inferred from the Ca II emission lines is likely an overestimate (Hartmann et al. 2011) and it is the only value in the literature close to the accretion rate found from our analysis. In the case of an instantaneous full disruption, the accretion rate will be even much higher since sufficient fragments will be generated in mutual collisions (e.g., Li et al. 2021; Brouwers et al. 2022). Details of such an extensive accretion process, which is out of the scope of this study, still need to be clarified in the future.

Most of the observed accretion rates in polluted WD systems are significantly lower than the rate in our work. This can be attributed to the rarity of the relevant process. The percentage of polluted WD systems, which is about 25%–50% (Zuckerman et al. 2003; Koester et al. 2014), is roughly consistent with the estimation of the exoplanet systems in the Milky Way (Cassan et al. 2012). The accretion rate decreases slowly (Hollands et al. 2018; Chen et al. 2019) or remains relatively steady (Blouin & Xu 2022) throughout the whole cooling stage of WDs, implying that the materials are continuously supplied. This is hard to explain by a single asteroid disruption event but requires extended debris from the tidal disruption or interaction with an asteroid belt. The planets around WDs can be involved in these processes, i.e., they can act either as pollutants or as drivers of pollutants depending on their orbits. As mentioned previously, asteroid disruption models, which require an object at least as massive as that of Earth’s moon for pollution drivers (Veras & Rosengren 2023), can produce low accretion rates. When a planet plays the role of pollutant, the mass of the driver (perturber) should be equal or larger than that of the pollutant to deliver it to the tidal disruption radius. The absence of observations that are in line with the accretion rates for the partial tidal disruption of a planet suggests that the proposed mechanism might be a rare process. This is consistent

with the argument that the pollution resulting from the tidal disruption of a planet is rare compared to the pollution from small bodies such as asteroids (Veras et al. 2024).

Moreover, it is worth noting that the interaction between the accreted materials and the WD may produce X-ray emission. The gravitational potential energy of the accreted material can be transformed into X-rays in the process. The corresponding X-ray luminosity can be expressed as (Cunningham et al. 2022)

$$L_X = A \frac{1}{2} \frac{GM_{\text{WD}} \dot{m}}{R_{\text{WD}}}, \quad (8)$$

where  $A = 0.5_{-0.4}^{+0.3}$  is a constant relevant to plasma cooling. It is usually assumed that half of the energy will be absorbed by the star and another half will be emitted in X-rays, which leads to the factor of 1/2 in the expression. Taken  $M_{\text{WD}} = 0.6M_{\odot}$ ,  $R_{\text{WD}} = 0.0129R_{\odot}$ ,  $A = 0.5$ , and  $\dot{m} = 10^{14} - 10^{18} \text{ g s}^{-1}$ , we have an X-ray luminosity of  $L_X = 2.2 \times 10^{30} - 2.2 \times 10^{34} \text{ erg s}^{-1}$ . These X-ray luminosities are exceptionally high and exceed the expected luminosity for a WD accreting material from an MS companion ( $\sim 10^{29} - 10^{33} \text{ erg s}^{-1}$ , Cunningham et al. 2022). This would be easier to observe than the previous X-ray observations of the WD accretion process. The lack of previous detections of these phenomena further implies that the proposed process is rare.

#### 5.4. Other forces that affect the clump evolution

Other nongravitational effects such as the Poynting-Robertson drag, the Yarkovsky effect, the Alfvén-wave drag, and sublimation can affect the orbital evolution of the tidal debris. A study by Veras et al. (2014) shows that a ring of debris (centimeter-sized) can be formed during the tidal disruption of a rubble-pile asteroid. The effect of Poynting-Robertson drag on the micrometer-to-cm-sized particles could shrink and circularize the ring/disc effectively on a timescale ranging from years up to hundreds of millions of years, depending on the exact size of the debris and the age of the WD (Veras et al. 2015b). The collisional grind-down in the tidal disc (Wyatt et al. 2011) can facilitate the accretion of debris materials onto the WD due to the Poynting-Robertson drag force (Swan et al. 2021; Li et al. 2021; Brouwers et al. 2022). However, when the debris particles are much larger than a centimeter size, the Poynting-Robertson drag becomes ineffective, and instead the Yarkovsky effect dominates (Veras et al. 2015b, 2022). Generally, the accretion timescale of small sub-cm or sub-dm particles under the action of the radiative forces is as long as  $> 10^4 \text{ yr}$ .

It has also been argued that a pre-existing compact gaseous disc in the vicinity of a WD can facilitate the

circularization of the orbit of the tidal debris (Malamud et al. 2021; Brouwers et al. 2022) and small exo-Kuiper or exo-Oort like objects with a size of 0.1–10 km (Grishin & Veras 2019). The circularization timescale depends on the structure (mass and compactness) of the disc. In our study, we have assumed that the circumstellar environment is clean. If a massive gaseous disc exists before the planet is destroyed, the accretion of the clumps will be accelerated correspondingly.

In addition to the above evolutionary routes, other effects may also play a role in the long-term evolutionary processes. They include the direct capture of asteroids/fragments by the WD due to the scatter effect of the outer planet, the sublimation of debris material which occurs when the debris is close to the star, and the accretion of gas (Veras et al. 2015a; Brouwers et al. 2022), and the gravitational perturbation of outer planet (Li et al. 2021). The timescales of these effects are usually larger than  $10^4 \text{ yr}$ . For example, the fragments are accreted by the WD over several Myr under the influence of gravitational perturbation of a distant planet with a semi-major axis of 10 au (Li et al. 2021).

Alfvén-wave drag caused by the magnetic field of the WD can effectively circularize the orbit of circum-stellar debris discs (Zhang et al. 2021). Usually, the circularization timescale depends on the size of the debris. For larger particles, the timescale is longer than that of smaller ones. For example, a fragment of 1 cm would be circularized on a timescale of 10 yr, while a fragment of 10 km can be circularized on a timescale of  $10^7 \text{ yr}$  (Zhang et al. 2021).

In our framework, the fragments generated during the partial disruption range from tiny dust to macroscopic asteroids. As mentioned previously, the dynamics of micrometer-to-centimeter particles could be affected by radiative force due to the Poynting-Robertson drag and Yarkovsky effect (Veras et al. 2015b). However, it is hard to estimate the exact mass fraction of these small particles. On the other hand, according to Malamud & Perets (2020a), there are at least two factors that prevent the formation of large amounts of dusty materials. First, small particles can coagulate into much larger fragments when they are gravitationally self-confined, which should be orders of magnitude larger than the sizes relevant to either the Poynting-Robertson drag or the Yarkovsky effect. Second, the particles lie well within the gravitational potential of their parent fragments (which are much larger) even if they are produced during the partial disruption process. Thus the dominant force is still gravitational for them, but not the Poynting-Robertson drag. Dusty particles could be formed via the collisional grinddown in a tidal disc (Wy-



att et al. 2011), but the collisions are unlikely to occur at the early stage of the disruption. Since the older fragments lose their angular momentum on a timescale of several orbital periods due to perturbation from the remnant planet, it is hard to form a disc before the complete destruction of the planet. Therefore, the fragments are essentially largely unaffected by radiation effects.

The perturbation of the outer planet and other non-gravitational effects such as the Poynting-Robertson drag, the Yarkovsky effect, the Alfvén-wave drag, and sublimation may play a significant role when the inner planet is completely destroyed. Collisional cascade in the tidal disc formed after the complete destruction can produce a larger number of small dusty particles on a long evolutionary timescale (Wyatt et al. 2011). As a result, nongravitational effects such as the Poynting-Robertson drag, the Yarkovsky effect, and the Alfvén-wave drag could be significant. The perturbation of the outer planet on the tidal debris disc may also be long-term effect (Li et al. 2021). To summarize, the accretion is likely to proceed under the combined effects of these channels. Each mechanism may play a different role at different stages according to the detailed condition of the system. But generally, at the early stages of the partial disruption, the contribution of these nongravitational effects on the accretion is small as compared with the gravitational perturbation from the remnant planet itself.

## 6. CONCLUSIONS

In this study, we investigate the impact of gravitational perturbation on the accretion of tidal debris in the case of partial tidal disruption. A triple system composed of a WD, a rocky planet in the inner orbit, and a Jupiter-like planet in the outer orbit is considered. The orbital parameters of the system evolve under the influence of secular effects such as the Kozai-Lidov mechanism. The eccentricity of the inner orbit planet can be excited to extremely high values so that its periastron distance decreases correspondingly, resulting in a partial disruption of the inner orbit planet. The surface material of the planet is stripped off but the main body can still survive. The partial disruption can occur repeatedly over a few thousands of years. The surviving portion of the planet loses its mass every time it passes through the periastron, the rate of which depends on the initial orbital configuration of the system and the planet's structure. A consequence of the mass loss is that the percentage of iron composition and mean density of the remnant planet increases, which leads the planet's core to finally become an iron-rich or pure iron object.

For the clumps generated during a partial disruption, gravitational perturbation from the remnant planet is a dominant force in the evolution. The clumps lose their angular momentum on a short timescale and finally collide with the WD. Again, the process is governed by the orbital configuration of the system and the planet's structure. Other nongravitational effects (the Poynting-Robertson effect, the Yarkovsky effect, the Alfvén-wave drag, and sublimation) can be neglected at early stages. However, gravitational perturbation becomes weaker and weaker with the decrease of the remnant planet mass. It may finally diminish if the remnant planet is destroyed completely. The collisional grind-down in the tidal disc formed later in the disruption can facilitate dust formation. It makes the nongravitational effects significant at late stages.

The proposed mechanism in the work can produce a high accretion rate in the range of  $\sim 10^{14}$ – $10^{18}$  g s<sup>-1</sup>. The lack of observations of such intense accretion episodes implies that the proposed mechanism in the work might be a rare process. If such intense accretion events could be observed by X-ray telescopes in the future, they would provide conclusive evidence of a partial disruption of planets around WDs.

## 7. ACKNOWLEDGMENTS

We would like to thank the anonymous referee for helpful suggestions that led to a significant improvement of our work. This study was supported by the Natural Science Foundation of Xinjiang Uygur Autonomous Region (Nos. 2022D01A363, 2023D01E20), the National Natural Science Foundation of China (Grant Nos. 12288102, 12033001, 12273028, 12041304, 12233002, 12041306), the Major Science and Technology Program of Xinjiang Uygur Autonomous Region (Nos. 2022A03013-1, 2022A03013-3), the National SKA Program of China No. 2020SKA0120300, the National Key R&D Program of China (2021YFA0718500), the Youth Innovations and Talents Project of Shandong Provincial Colleges and Universities (Grant No. 201909118), the Tianshan Talents Training Program (2023TSYCTD0013). YFH acknowledges the support from the Xinjiang Tianchi Program. AK acknowledges the support from the Tianchi Talents Project of Xinjiang Uygur Autonomous Region and the special research assistance project of the Chinese Academy of Sciences (CAS). This work was also supported by the Operation, Maintenance and Upgrading Fund for Astronomical Telescopes and Facility Instruments, budgeted from the Ministry of Finance of China (MOF) and administrated by the CAS, the Urumqi Nanshan Astronomy



and Deep Space Exploration Observation and Research Station of Xinjiang (XJYWZ2303).

*Software:* SciPy (Virtanen et al. 2020), Matplotlib (Hunter 2007), NumPy (van der Walt et al. 2011) .

## REFERENCES

- Adams, F. C., & Laughlin, G. 2003, *Icarus*, 163, 290, doi: [10.1016/S0019-1035\(03\)00081-2](https://doi.org/10.1016/S0019-1035(03)00081-2)
- Antoniadou, K. I., & Veras, D. 2016, *MNRAS*, 463, 4108, doi: [10.1093/mnras/stw2264](https://doi.org/10.1093/mnras/stw2264)
- Antonini, F., Chatterjee, S., Rodriguez, C. L., et al. 2016, *ApJ*, 816, 65, doi: [10.3847/0004-637X/816/2/65](https://doi.org/10.3847/0004-637X/816/2/65)
- Antonini, F., Murray, N., & Mikkola, S. 2014, *ApJ*, 781, 45, doi: [10.1088/0004-637X/781/1/45](https://doi.org/10.1088/0004-637X/781/1/45)
- Antonini, F., & Perets, H. B. 2012, *ApJ*, 757, 27, doi: [10.1088/0004-637X/757/1/27](https://doi.org/10.1088/0004-637X/757/1/27)
- Armstrong, D. J., Lopez, T. A., Adibekyan, V., et al. 2020, *Nature*, 583, 39, doi: [10.1038/s41586-020-2421-7](https://doi.org/10.1038/s41586-020-2421-7)
- Bareither, C. A., Edil, T. B., Benson, C. H., & Mickelson, D. M. 2008, *Journal of Geotechnical and Geoenvironmental Engineering*, 134, 1476, doi: [10.1061/\(ASCE\)1090-0241\(2008\)134:10\(1476\)](https://doi.org/10.1061/(ASCE)1090-0241(2008)134:10(1476))
- Bhaskar, H., Li, G., Hadden, S., Payne, M. J., & Holman, M. J. 2021, *AJ*, 161, 48, doi: [10.3847/1538-3881/abcbfc](https://doi.org/10.3847/1538-3881/abcbfc)
- Blackman, J. W., Beaulieu, J. P., Bennett, D. P., et al. 2021, *Nature*, 598, 272, doi: [10.1038/s41586-021-03869-6](https://doi.org/10.1038/s41586-021-03869-6)
- Blouin, S., & Xu, S. 2022, *MNRAS*, 510, 1059, doi: [10.1093/mnras/stab3446](https://doi.org/10.1093/mnras/stab3446)
- Bode, J. N., & Wegg, C. 2014, *MNRAS*, 438, 573, doi: [10.1093/mnras/stt2227](https://doi.org/10.1093/mnras/stt2227)
- Bonsor, A., Mustill, A. J., & Wyatt, M. C. 2011, *MNRAS*, 414, 930, doi: [10.1111/j.1365-2966.2011.18524.x](https://doi.org/10.1111/j.1365-2966.2011.18524.x)
- Bonsor, A., & Veras, D. 2015, *MNRAS*, 454, 53, doi: [10.1093/mnras/stv1913](https://doi.org/10.1093/mnras/stv1913)
- Brouwers, M. G., Bonsor, A., & Malamud, U. 2022, *MNRAS*, 509, 2404, doi: [10.1093/mnras/stab3009](https://doi.org/10.1093/mnras/stab3009)
- Budaj, J., Maliuk, A., & Hubeny, I. 2022, *A&A*, 660, A72, doi: [10.1051/0004-6361/202141924](https://doi.org/10.1051/0004-6361/202141924)
- Carrera, D., Raymond, S. N., & Davies, M. B. 2019, *A&A*, 629, L7, doi: [10.1051/0004-6361/201935744](https://doi.org/10.1051/0004-6361/201935744)
- Cassan, A., Kubas, D., Beaulieu, J. P., et al. 2012, *Nature*, 481, 167, doi: [10.1038/nature10684](https://doi.org/10.1038/nature10684)
- Chambers, J. E. 1999, *MNRAS*, 304, 793, doi: [10.1046/j.1365-8711.1999.02379.x](https://doi.org/10.1046/j.1365-8711.1999.02379.x)
- Chen, D.-C., Zhou, J.-L., Xie, J.-W., et al. 2019, *Nature Astronomy*, 3, 69, doi: [10.1038/s41550-018-0609-7](https://doi.org/10.1038/s41550-018-0609-7)
- Chu, Y.-H., Toalá, J. A., Guerrero, M. A., et al. 2021, *ApJ*, 910, 119, doi: [10.3847/1538-4357/abe5a5](https://doi.org/10.3847/1538-4357/abe5a5)
- Coughlin, E. R., & Nixon, C. J. 2022, *MNRAS*, 517, L26, doi: [10.1093/mnras/slac106](https://doi.org/10.1093/mnras/slac106)
- Cummings, J. D., Kalirai, J. S., Tremblay, P. E., Ramirez-Ruiz, E., & Choi, J. 2018, *ApJ*, 866, 21, doi: [10.3847/1538-4357/aadfd6](https://doi.org/10.3847/1538-4357/aadfd6)
- Cunningham, T., Wheatley, P. J., Tremblay, P.-E., et al. 2022, *Nature*, 602, 219, doi: [10.1038/s41586-021-04300-w](https://doi.org/10.1038/s41586-021-04300-w)
- Debes, J. H., & Sigurdsson, S. 2002, *ApJ*, 572, 556, doi: [10.1086/340291](https://doi.org/10.1086/340291)
- Debes, J. H., Walsh, K. J., & Stark, C. 2012, *ApJ*, 747, 148, doi: [10.1088/0004-637X/747/2/148](https://doi.org/10.1088/0004-637X/747/2/148)
- Duvvuri, G. M., Redfield, S., & Veras, D. 2020, *ApJ*, 893, 166, doi: [10.3847/1538-4357/ab7fa0](https://doi.org/10.3847/1538-4357/ab7fa0)
- Eggleton, P., & Kiseleva, L. 1995, *ApJ*, 455, 640, doi: [10.1086/176611](https://doi.org/10.1086/176611)
- Estrada-Dorado, S., Guerrero, M. A., Toalá, J. A., et al. 2023, *ApJL*, 944, L46, doi: [10.3847/2041-8213/acba7e](https://doi.org/10.3847/2041-8213/acba7e)
- Faber, J. A., Rasio, F. A., & Willems, B. 2005, *Icarus*, 175, 248, doi: [10.1016/j.icarus.2004.10.021](https://doi.org/10.1016/j.icarus.2004.10.021)
- Farihi, J. 2016, *NewAR*, 71, 9, doi: [10.1016/j.newar.2016.03.001](https://doi.org/10.1016/j.newar.2016.03.001)
- Farihi, J., Gänsicke, B. T., Wyatt, M. C., et al. 2012, *MNRAS*, 424, 464, doi: [10.1111/j.1365-2966.2012.21215.x](https://doi.org/10.1111/j.1365-2966.2012.21215.x)
- Farihi, J., Hermes, J. J., Marsh, T. R., et al. 2022, *MNRAS*, 511, 1647, doi: [10.1093/mnras/stab3475](https://doi.org/10.1093/mnras/stab3475)
- Frewen, S. F. N., & Hansen, B. M. S. 2014, *MNRAS*, 439, 2442, doi: [10.1093/mnras/stu097](https://doi.org/10.1093/mnras/stu097)
- Gänsicke, B. T., Schreiber, M. R., Toloza, O., et al. 2019, *Nature*, 576, 61, doi: [10.1038/s41586-019-1789-8](https://doi.org/10.1038/s41586-019-1789-8)
- Geng, J. J., Huang, Y. F., & Lu, T. 2015, *ApJ*, 804, 21, doi: [10.1088/0004-637X/804/1/21](https://doi.org/10.1088/0004-637X/804/1/21)
- Girven, J., Brinkworth, C. S., Farihi, J., et al. 2012, *ApJ*, 749, 154, doi: [10.1088/0004-637X/749/2/154](https://doi.org/10.1088/0004-637X/749/2/154)
- Goffo, E., Gandolfi, D., Egger, J. A., et al. 2023, *ApJL*, 955, L3, doi: [10.3847/2041-8213/ace0c7](https://doi.org/10.3847/2041-8213/ace0c7)
- Gouliniski, N., & Ribak, E. N. 2018, *MNRAS*, 473, 1589, doi: [10.1093/mnras/stx2506](https://doi.org/10.1093/mnras/stx2506)
- Granvik, M., Morbidelli, A., Jedicke, R., et al. 2016, *Nature*, 530, 303, doi: [10.1038/nature16934](https://doi.org/10.1038/nature16934)
- Grishin, E., & Veras, D. 2019, *MNRAS*, 489, 168, doi: [10.1093/mnras/stz2148](https://doi.org/10.1093/mnras/stz2148)
- Guidry, J. A., Vanderbosch, Z. P., Hermes, J. J., et al. 2021, *ApJ*, 912, 125, doi: [10.3847/1538-4357/abee68](https://doi.org/10.3847/1538-4357/abee68)
- Guillochon, J., & Ramirez-Ruiz, E. 2013, *ApJ*, 767, 25, doi: [10.1088/0004-637X/767/1/25](https://doi.org/10.1088/0004-637X/767/1/25)
- Guillochon, J., Ramirez-Ruiz, E., & Lin, D. 2011, *ApJ*, 732, 74, doi: [10.1088/0004-637X/732/2/74](https://doi.org/10.1088/0004-637X/732/2/74)

- Hamers, A. S., Perets, H. B., Thompson, T. A., & Neunteufel, P. 2022, *ApJ*, 925, 178, doi: [10.3847/1538-4357/ac400b](https://doi.org/10.3847/1538-4357/ac400b)
- Hamers, A. S., & Portegies Zwart, S. F. 2016, *MNRAS*, 462, L84, doi: [10.1093/mnrasl/slwl134](https://doi.org/10.1093/mnrasl/slwl134)
- Harrison, J. H. D., Bonsor, A., Kama, M., et al. 2021, *MNRAS*, 504, 2853, doi: [10.1093/mnras/stab736](https://doi.org/10.1093/mnras/stab736)
- Hartmann, S., Nagel, T., Rauch, T., & Werner, K. 2011, *A&A*, 530, A7, doi: [10.1051/0004-6361/201116625](https://doi.org/10.1051/0004-6361/201116625)
- He, M. Y., & Petrovich, C. 2018, *MNRAS*, 474, 20, doi: [10.1093/mnras/stx2718](https://doi.org/10.1093/mnras/stx2718)
- Hills, J. G. 1975, *Nature*, 254, 295, doi: [10.1038/254295a0](https://doi.org/10.1038/254295a0)
- Hogg, M. A., Cutter, R., & Wynn, G. A. 2021, *MNRAS*, 500, 2986, doi: [10.1093/mnras/staa3316](https://doi.org/10.1093/mnras/staa3316)
- Hollands, M. A., Gänsicke, B. T., & Koester, D. 2018, *MNRAS*, 477, 93, doi: [10.1093/mnras/sty592](https://doi.org/10.1093/mnras/sty592)
- Huang, Y. F., & Yu, Y. B. 2017, *ApJ*, 848, 115, doi: [10.3847/1538-4357/aa8b63](https://doi.org/10.3847/1538-4357/aa8b63)
- Hunter, J. D. 2007, *Computing in Science and Engineering*, 9, 90, doi: [10.1109/MCSE.2007.55](https://doi.org/10.1109/MCSE.2007.55)
- Jura, M. 2003, *ApJL*, 584, L91, doi: [10.1086/374036](https://doi.org/10.1086/374036)
- Katz, B., & Dong, S. 2012, arXiv e-prints, arXiv:1211.4584. <https://arxiv.org/abs/1211.4584>
- Klein, B. L., Doyle, A. E., Zuckerman, B., et al. 2021, *ApJ*, 914, 61, doi: [10.3847/1538-4357/abe40b](https://doi.org/10.3847/1538-4357/abe40b)
- Kleinman, S. J., Kepler, S. O., Koester, D., et al. 2013, *ApJS*, 204, 5, doi: [10.1088/0067-0049/204/1/5](https://doi.org/10.1088/0067-0049/204/1/5)
- Koester, D. 2009, *A&A*, 498, 517, doi: [10.1051/0004-6361/200811468](https://doi.org/10.1051/0004-6361/200811468)
- Koester, D., Gänsicke, B. T., & Farihi, J. 2014, *A&A*, 566, A34, doi: [10.1051/0004-6361/201423691](https://doi.org/10.1051/0004-6361/201423691)
- Kozai, Y. 1962, *AJ*, 67, 591, doi: [10.1086/108790](https://doi.org/10.1086/108790)
- Kratter, K. M., & Perets, H. B. 2012, *ApJ*, 753, 91, doi: [10.1088/0004-637X/753/1/91](https://doi.org/10.1088/0004-637X/753/1/91)
- Kremer, K., D'Orazio, D. J., Samsing, J., Chatterjee, S., & Rasio, F. A. 2019, *ApJ*, 885, 2, doi: [10.3847/1538-4357/ab44d1](https://doi.org/10.3847/1538-4357/ab44d1)
- Kurban, A., Geng, J.-J., & Huang, Y.-F. 2019, in *American Institute of Physics Conference Series*, Vol. 2127, Xiamen-CUSTIPEN Workshop on the Equation of State of Dense Neutron-Rich Matter in the Era of Gravitational Wave Astronomy, 020027, doi: [10.1063/1.5117817](https://doi.org/10.1063/1.5117817)
- Kurban, A., Geng, J.-J., Huang, Y.-F., Zong, H.-S., & Gong, H. 2020, *ApJ*, 890, 41, doi: [10.3847/1538-4357/ab698b](https://doi.org/10.3847/1538-4357/ab698b)
- Kunitomo, M., Ikoma, M., Sato, B., Katsuta, Y., & Ida, S. 2011, *ApJ*, 737, 66, doi: [10.1088/0004-637X/737/2/66](https://doi.org/10.1088/0004-637X/737/2/66)
- Kurban, A., Zhou, X., Wang, N., et al. 2023, *MNRAS*, 522, 4265, doi: [10.1093/mnras/stad1260](https://doi.org/10.1093/mnras/stad1260)
- . 2024, *A&A*, 686, A87, doi: [10.1051/0004-6361/202347828](https://doi.org/10.1051/0004-6361/202347828)
- Kurban, A., Huang, Y.-F., Geng, J.-J., et al. 2022, *ApJ*, 928, 94, doi: [10.3847/1538-4357/ac558f](https://doi.org/10.3847/1538-4357/ac558f)
- Lam, K. W. F., Csizmadia, S., Astudillo-Defru, N., et al. 2021, *Science*, 374, 1271, doi: [10.1126/science.aay3253](https://doi.org/10.1126/science.aay3253)
- Law-Smith, J. A. P., Coulter, D. A., Guillochon, J., Mockler, B., & Ramirez-Ruiz, E. 2020, *ApJ*, 905, 141, doi: [10.3847/1538-4357/abc489](https://doi.org/10.3847/1538-4357/abc489)
- Li, D., Mustill, A. J., & Davies, M. B. 2021, *MNRAS*, 508, 5671, doi: [10.1093/mnras/stab2949](https://doi.org/10.1093/mnras/stab2949)
- Lidov, M. L. 1962, *Planetary and Space Science*, 9, 719, doi: [10.1016/0032-0633\(62\)90129-0](https://doi.org/10.1016/0032-0633(62)90129-0)
- Liu, S.-F., Guillochon, J., Lin, D. N. C., & Ramirez-Ruiz, E. 2013, *ApJ*, 762, 37, doi: [10.1088/0004-637X/762/1/37](https://doi.org/10.1088/0004-637X/762/1/37)
- Luhman, K. L., Burgasser, A. J., & Bochanski, J. J. 2011, *ApJL*, 730, L9, doi: [10.1088/2041-8205/730/1/L9](https://doi.org/10.1088/2041-8205/730/1/L9)
- Malamud, U., Grishin, E., & Brouwers, M. 2021, *MNRAS*, 501, 3806, doi: [10.1093/mnras/staa3940](https://doi.org/10.1093/mnras/staa3940)
- Malamud, U., & Perets, H. B. 2020a, *MNRAS*, 492, 5561, doi: [10.1093/mnras/staa142](https://doi.org/10.1093/mnras/staa142)
- . 2020b, *MNRAS*, 493, 698, doi: [10.1093/mnras/staa143](https://doi.org/10.1093/mnras/staa143)
- Malavolta, L., Mayo, A. W., Louden, T., et al. 2018, *AJ*, 155, 107, doi: [10.3847/1538-3881/aaa5b5](https://doi.org/10.3847/1538-3881/aaa5b5)
- Maldonado, R. F., Villaver, E., Mustill, A. J., & Chávez, M. 2022, *MNRAS*, 512, 104, doi: [10.1093/mnras/stac481](https://doi.org/10.1093/mnras/stac481)
- Maldonado, R. F., Villaver, E., Mustill, A. J., Chavez, M., & Bertone, E. 2020a, *MNRAS*, 497, 4091, doi: [10.1093/mnras/staa2237](https://doi.org/10.1093/mnras/staa2237)
- . 2020b, *MNRAS*, 499, 1854, doi: [10.1093/mnras/staa2946](https://doi.org/10.1093/mnras/staa2946)
- Maldonado, R. F., Villaver, E., Mustill, A. J., Chávez, M., & Bertone, E. 2021, *MNRAS*, 501, L43, doi: [10.1093/mnrasl/slaa193](https://doi.org/10.1093/mnrasl/slaa193)
- Manser, C. J., Gänsicke, B. T., Eggl, S., et al. 2019, *Science*, 364, 66, doi: [10.1126/science.aat5330](https://doi.org/10.1126/science.aat5330)
- Mardling, R. A., & Aarseth, S. J. 2001, *MNRAS*, 321, 398, doi: [10.1046/j.1365-8711.2001.03974.x](https://doi.org/10.1046/j.1365-8711.2001.03974.x)
- Metzger, B. D., Rafikov, R. R., & Bochkarev, K. V. 2012, *MNRAS*, 423, 505, doi: [10.1111/j.1365-2966.2012.20895.x](https://doi.org/10.1111/j.1365-2966.2012.20895.x)
- Muñoz, D. J., & Petrovich, C. 2020, *ApJL*, 904, L3, doi: [10.3847/2041-8213/abc564](https://doi.org/10.3847/2041-8213/abc564)
- Mukai, K. 2017, *PASP*, 129, 062001, doi: [10.1088/1538-3873/aa6736](https://doi.org/10.1088/1538-3873/aa6736)
- Mustill, A. J., Davies, M. B., Blunt, S., & Howard, A. 2022, *MNRAS*, 509, 3616, doi: [10.1093/mnras/stab3174](https://doi.org/10.1093/mnras/stab3174)
- Mustill, A. J., Veras, D., & Villaver, E. 2014, *MNRAS*, 437, 1404, doi: [10.1093/mnras/stt1973](https://doi.org/10.1093/mnras/stt1973)
- Mustill, A. J., & Villaver, E. 2012, *ApJ*, 761, 121, doi: [10.1088/0004-637X/761/2/121](https://doi.org/10.1088/0004-637X/761/2/121)

- Mustill, A. J., Villaver, E., Veras, D., Gänsicke, B. T., & Bonsor, A. 2018, *MNRAS*, 476, 3939, doi: [10.1093/mnras/sty446](https://doi.org/10.1093/mnras/sty446)
- Nagasawa, M., & Ida, S. 2011, *ApJ*, 742, 72, doi: [10.1088/0004-637X/742/2/72](https://doi.org/10.1088/0004-637X/742/2/72)
- Naoz, S. 2016, *ARA&A*, 54, 441, doi: [10.1146/annurev-astro-081915-023315](https://doi.org/10.1146/annurev-astro-081915-023315)
- Naoz, S., Farr, W. M., Lithwick, Y., Rasio, F. A., & Teyssandier, J. 2011, *Nature*, 473, 187, doi: [10.1038/nature10076](https://doi.org/10.1038/nature10076)
- Naponiello, L., Mancini, L., Sozzetti, A., et al. 2023, *Nature*, 622, 255, doi: [10.1038/s41586-023-06499-2](https://doi.org/10.1038/s41586-023-06499-2)
- O'Connor, C. E., & Lai, D. 2020, *MNRAS*, 498, 4005, doi: [10.1093/mnras/staa2645](https://doi.org/10.1093/mnras/staa2645)
- O'Connor, C. E., Liu, B., & Lai, D. 2021, *MNRAS*, 501, 507, doi: [10.1093/mnras/staa3723](https://doi.org/10.1093/mnras/staa3723)
- O'Connor, C. E., Teyssandier, J., & Lai, D. 2022, *MNRAS*, 513, 4178, doi: [10.1093/mnras/stac1189](https://doi.org/10.1093/mnras/stac1189)
- Paquette, C., Pelletier, C., Fontaine, G., & Michaud, G. 1986, *ApJS*, 61, 197, doi: [10.1086/191112](https://doi.org/10.1086/191112)
- Perets, H. B., & Kratter, K. M. 2012, *ApJ*, 760, 99, doi: [10.1088/0004-637X/760/2/99](https://doi.org/10.1088/0004-637X/760/2/99)
- Petrovich, C., & Muñoz, D. J. 2017, *ApJ*, 834, 116, doi: [10.3847/1538-4357/834/2/116](https://doi.org/10.3847/1538-4357/834/2/116)
- Pohl, L., & Britt, D. T. 2020, *M&PS*, 55, 962, doi: [10.1111/maps.13449](https://doi.org/10.1111/maps.13449)
- Rafikov, R. R. 2011a, *ApJL*, 732, L3, doi: [10.1088/2041-8205/732/1/L3](https://doi.org/10.1088/2041-8205/732/1/L3)
- . 2011b, *MNRAS*, 416, L55, doi: [10.1111/j.1745-3933.2011.01096.x](https://doi.org/10.1111/j.1745-3933.2011.01096.x)
- Rees, M. J. 1988, *Nature*, 333, 523, doi: [10.1038/333523a0](https://doi.org/10.1038/333523a0)
- Rossi, E. M., Stone, N. C., Law-Smith, J. A. P., et al. 2021, *SSRv*, 217, 40, doi: [10.1007/s11214-021-00818-7](https://doi.org/10.1007/s11214-021-00818-7)
- Ryu, T., Krolik, J., Piran, T., & Noble, S. C. 2020, *ApJ*, 904, 100, doi: [10.3847/1538-4357/abb3ce](https://doi.org/10.3847/1538-4357/abb3ce)
- Sato, B., Izumiura, H., Toyota, E., et al. 2008, *PASJ*, 60, 539, doi: [10.1093/pasj/60.3.539](https://doi.org/10.1093/pasj/60.3.539)
- Seager, S., Kuchner, M., Hier-Majumder, C. A., & Militzer, B. 2007, *ApJ*, 669, 1279, doi: [10.1086/521346](https://doi.org/10.1086/521346)
- Smith, R. F., Fratanduono, D. E., Braun, D. G., et al. 2018, *Nature Astronomy*, 2, 452, doi: [10.1038/s41550-018-0437-9](https://doi.org/10.1038/s41550-018-0437-9)
- Stephan, A. P., Naoz, S., & Gaudi, B. S. 2021, *ApJ*, 922, 4, doi: [10.3847/1538-4357/ac22a9](https://doi.org/10.3847/1538-4357/ac22a9)
- Stephan, A. P., Naoz, S., & Zuckerman, B. 2017, *ApJL*, 844, L16, doi: [10.3847/2041-8213/aa7cf3](https://doi.org/10.3847/2041-8213/aa7cf3)
- Stock, K., Veras, D., Cai, M. X., Spurzem, R., & Portegies Zwart, S. 2022, *MNRAS*, 512, 2460, doi: [10.1093/mnras/stac602](https://doi.org/10.1093/mnras/stac602)
- Swan, A., Kenyon, S. J., Farihi, J., et al. 2021, *MNRAS*, 506, 432, doi: [10.1093/mnras/stab1738](https://doi.org/10.1093/mnras/stab1738)
- Thorsett, S. E., Arzoumanian, Z., & Taylor, J. H. 1993, *ApJL*, 412, L33, doi: [10.1086/186933](https://doi.org/10.1086/186933)
- Toonen, S., Boekholt, T. C. N., & Portegies Zwart, S. 2022, *A&A*, 661, A61, doi: [10.1051/0004-6361/202141991](https://doi.org/10.1051/0004-6361/202141991)
- van der Walt, S., Colbert, S. C., & Varoquaux, G. 2011, *Computing in Science and Engineering*, 13, 22, doi: [10.1109/MCSE.2011.37](https://doi.org/10.1109/MCSE.2011.37)
- Vanderbosch, Z., Hermes, J. J., Dennihy, E., et al. 2020, *ApJ*, 897, 171, doi: [10.3847/1538-4357/ab9649](https://doi.org/10.3847/1538-4357/ab9649)
- Vanderbosch, Z. P., Rappaport, S., Guidry, J. A., et al. 2021, *ApJ*, 917, 41, doi: [10.3847/1538-4357/ac0822](https://doi.org/10.3847/1538-4357/ac0822)
- Vanderburg, A., Johnson, J. A., Rappaport, S., et al. 2015, *Nature*, 526, 546, doi: [10.1038/nature15527](https://doi.org/10.1038/nature15527)
- Vanderburg, A., Rappaport, S. A., Xu, S., et al. 2020, *Nature*, 585, 363, doi: [10.1038/s41586-020-2713-y](https://doi.org/10.1038/s41586-020-2713-y)
- Veras, D. 2016a, *MNRAS*, 463, 2958, doi: [10.1093/mnras/stw2170](https://doi.org/10.1093/mnras/stw2170)
- . 2016b, *Royal Society Open Science*, 3, 150571, doi: [10.1098/rsos.150571](https://doi.org/10.1098/rsos.150571)
- . 2020, *MNRAS*, 493, 4692, doi: [10.1093/mnras/staa625](https://doi.org/10.1093/mnras/staa625)
- . 2021, in *Oxford Research Encyclopedia of Planetary Science*, 1, doi: [10.1093/acrefore/9780190647926.013.238](https://doi.org/10.1093/acrefore/9780190647926.013.238)
- Veras, D., Birader, Y., & Zaman, U. 2022, *MNRAS*, 510, 3379, doi: [10.1093/mnras/stab3490](https://doi.org/10.1093/mnras/stab3490)
- Veras, D., Eggl, S., & Gänsicke, B. T. 2015a, *MNRAS*, 452, 1945, doi: [10.1093/mnras/stv1417](https://doi.org/10.1093/mnras/stv1417)
- Veras, D., & Fuller, J. 2020, *MNRAS*, 492, 6059, doi: [10.1093/mnras/staa309](https://doi.org/10.1093/mnras/staa309)
- Veras, D., Georgakarakos, N., Dobbs-Dixon, I., & Gänsicke, B. T. 2017, *MNRAS*, 465, 2053, doi: [10.1093/mnras/stw2699](https://doi.org/10.1093/mnras/stw2699)
- Veras, D., Georgakarakos, N., Gänsicke, B. T., & Dobbs-Dixon, I. 2018, *MNRAS*, 481, 2180, doi: [10.1093/mnras/sty2409](https://doi.org/10.1093/mnras/sty2409)
- Veras, D., Leinhardt, Z. M., Bonsor, A., & Gänsicke, B. T. 2014, *MNRAS*, 445, 2244, doi: [10.1093/mnras/stu1871](https://doi.org/10.1093/mnras/stu1871)
- Veras, D., Leinhardt, Z. M., Eggl, S., & Gänsicke, B. T. 2015b, *MNRAS*, 451, 3453, doi: [10.1093/mnras/stv1195](https://doi.org/10.1093/mnras/stv1195)
- Veras, D., Mustill, A. J., & Bonsor, A. 2024, *Reviews in Mineralogy and Geochemistry*, 90, 141, doi: [10.2138/rmg.2024.90.05](https://doi.org/10.2138/rmg.2024.90.05)
- Veras, D., Mustill, A. J., Bonsor, A., & Wyatt, M. C. 2013, *MNRAS*, 431, 1686, doi: [10.1093/mnras/stt289](https://doi.org/10.1093/mnras/stt289)
- Veras, D., Mustill, A. J., Gänsicke, B. T., et al. 2016, *MNRAS*, 458, 3942, doi: [10.1093/mnras/stw476](https://doi.org/10.1093/mnras/stw476)
- Veras, D., & Rosengren, A. J. 2023, *MNRAS*, 519, 6257, doi: [10.1093/mnras/stad130](https://doi.org/10.1093/mnras/stad130)

- Veras, D., & Wolszczan, A. 2019, *MNRAS*, 488, 153, doi: [10.1093/mnras/stz1721](https://doi.org/10.1093/mnras/stz1721)
- Veras, D., Efroimsky, M., Makarov, V. V., et al. 2019, *MNRAS*, 486, 3831, doi: [10.1093/mnras/stz965](https://doi.org/10.1093/mnras/stz965)
- Villaver, E., & Livio, M. 2009, *ApJL*, 705, L81, doi: [10.1088/0004-637X/705/1/L81](https://doi.org/10.1088/0004-637X/705/1/L81)
- Villaver, E., Livio, M., Mustill, A. J., & Siess, L. 2014, *ApJ*, 794, 3, doi: [10.1088/0004-637X/794/1/3](https://doi.org/10.1088/0004-637X/794/1/3)
- Virtanen, P., Gommers, R., Oliphant, T. E., et al. 2020, *Nature Methods*, 17, 261, doi: [10.1038/s41592-019-0686-2](https://doi.org/10.1038/s41592-019-0686-2)
- Wyatt, M. C., Clarke, C. J., & Booth, M. 2011, *Celestial Mechanics and Dynamical Astronomy*, 111, 1, doi: [10.1007/s10569-011-9345-3](https://doi.org/10.1007/s10569-011-9345-3)
- Wyatt, M. C., Farihi, J., Pringle, J. E., & Bonsor, A. 2014, *MNRAS*, 439, 3371, doi: [10.1093/mnras/stu183](https://doi.org/10.1093/mnras/stu183)
- Wyatt, M. C., Smith, R., Greaves, J. S., et al. 2007, *ApJ*, 658, 569, doi: [10.1086/510999](https://doi.org/10.1086/510999)
- Xu, S., Jura, M., Dufour, P., & Zuckerman, B. 2016, *ApJL*, 816, L22, doi: [10.3847/2041-8205/816/2/L22](https://doi.org/10.3847/2041-8205/816/2/L22)
- Zanazzi, J. J., & Ogilvie, G. I. 2020, *MNRAS*, 499, 5562, doi: [10.1093/mnras/staa3127](https://doi.org/10.1093/mnras/staa3127)
- Zhang, E., Naoz, S., & Will, C. M. 2023, arXiv e-prints, arXiv:2301.08271, doi: [10.48550/arXiv.2301.08271](https://doi.org/10.48550/arXiv.2301.08271)
- Zhang, Y., Liu, S.-F., & Lin, D. N. C. 2021, *ApJ*, 915, 91, doi: [10.3847/1538-4357/ac00ae](https://doi.org/10.3847/1538-4357/ac00ae)
- Zuckerman, B., Koester, D., Reid, I. N., & Hüensch, M. 2003, *ApJ*, 596, 477, doi: [10.1086/377492](https://doi.org/10.1086/377492)